Journal of Applied Electrochemistry **33**: 245–252, 2003.

Detection and characterization of molybdenum oxides formed during the initial stages of cobalt–molybdenum electrodeposition

E. GÓMEZ*, E. PELLICER and E. VALLÉS
Laboratori de Ciència i Tecnologia Electroquímica dels Materials (LCTEM), Departament Química Física. Facultat de Química. Universitat de Barcelona. Martí i Franquès, 1. 08028 Barcelona, Spain
*(*author for correspondence, fax: +34 93 4021231, e-mail: e.gomez@qf.ub.es)*

Received 19 August 2002; accepted in revised form 15 December 2002

Key words: cobalt–molybdenum, electrodeposition, induced codeposition, molybdenum oxides

Abstract

The initial stages of cobalt–molybdenum electrodeposition on a vitreous carbon electrode were studied to obtain information about the mechanism of cobalt–molybdenum induced codeposition. Solutions containing cobalt sulphate, sodium molybdate and sodium citrate at pH 6.6 were used. A first step in the mechanism of alloy deposition is proposed. This step takes into account the formation of molybdenum(IV) oxides over which Co–Mo alloy may be only deposited if sufficient potential is applied. Co–Mo electrodeposition occurs through an early stage involving low reduction current, related to the formation of molybdenum oxides, followed by a later stage in which the reduction current suddenly increases, corresponding to alloy codeposition. When a low potential is applied, a continuous coloured molybdenum oxide film is formed on the electrode and Co–Mo is not deposited. To induce the alloy deposition on the 'oxide film' it is necessary to apply more negative potentials than a threshold value, which depends on the composition of the electrolytic bath. By increasing molybdate concentration in solution, the 'threshold potential' shifts to more negative values. Intermediate molybdenum oxides were characterized using scanning electron microscopy (SEM), compositional analysis, Raman measurements and Auger and X-ray photoelectron spectroscopies.

1. Introduction

Alloys containing molybdenum are of interest because of their hardness, thermal and corrosion resistance and magnetic properties. They also offer good catalytic properties for hydrogen evolution [1–4]. Electrodeposition is a useful method to obtain these alloys. Molybdenum cannot be electrodeposited alone from aqueous solutions [5], but can be obtained by electrodeposition as an alloy, such as combined with an iron-group metal (induced codeposition).

Several studies have examined the induced codeposition mechanism between the molybdenum and an iron-group element and various hypotheses centred specially on Ni–Mo codeposition have been put forward [6–9]. Podlaha et al. extended the proposed sequence of steps for Ni–Mo codeposition [8, 9] to the codeposition of all iron group-molybdenum [10]. They suggested the formation of an intermediate, which involves an iron-group element that may act as a catalyst for the reduction of a proposed molybdenum oxide intermediate.

Previously, we studied the Co–Mo electrodeposition from a citrate-sulfate bath in order to obtain alloys that exhibit soft magnetic behaviour [11]. Baths with high cobalt(II)/molybdate ratios, greater than $[Co(II)]/[MoO_4^{2-}] = 6$, were used due to the great ability of the molybdenum to incorporate in the deposit. During the electrochemical study of the process two distinct responses were obtained in potentiostatic experiments depending on the applied potential. As a result of this unexpected behaviour, we decided, in the present work, to analyse the first stages of Co–Mo electrodeposition. This study aims to clarify the Co–Mo mechanism, by characterising the electrochemical response and the films produced in the initial stages of the reduction process. Improved knowledge of the deposition mechanism will facilitate the final objective of preparing Co–Mo deposits with desired magnetic properties.

2. Experimental details

Electrochemical measurements were taken from a conventional thermostatted three-electrode cell, using a microcomputer-controlled potentiostat/galvanostat (model 273, EG&G) or an Autolab with PGSTAT30 equipment and GPES software. The temperature was maintained at 25 °C. The chemicals used were $CoSO_4 \cdot 7H_2O$, $Na_2MoO_4 \cdot 2H_2O$ and $Na_3C_6H_5O_7 \cdot 2H_2O$, all of analytical grade. All solutions were freshly

prepared with water which was first doubly distilled and then treated with a Millipore Milli Q system. Citrate was always maintained at 0.2 mol dm^{-3}. The pH was adjusted to 6.6. Before each experiment the solutions were deaerated by argon bubbling and maintained under argon atmosphere during the recording of the experimental curves.

The working electrode used was a vitreous carbon (Metrohm) rod of 2 mm in diameter. It was polished to a mirror finish using alumina of distinct grades (3.75 and 1.87 μm) and cleaned ultrasonically for 2 min in water. The counter electrode was a platinum spiral. The reference was a Ag|AgCl|NaCl 1 mol dm^{-3} electrode mounted in a Luggin capillary containing 0.5 mol dm^{-3} Na_2SO_4 solution. All potentials are referred to this electrode.

Voltammetric experiments were carried out initially scanning in the negative direction. Only one cycle was run in each voltammetric experiment. Chronoamperometric experiments were done by stepping the potential from an initial value at which no process occurred to a value at which the reduction process occurred. Deposits were obtained under moderate stirring at 60 rpm.

The morphology of the deposits was examined with a Hitachi S 2300 or with a Leica Cambridge Stereoscan S-360 scanning electron microscopes. Elemental composition was determined using an X-ray analyser incorporated in the Leica equipment (EDS). For quantitative analysis, standards of pure molybdenum and pure cobalt, previously polished, were used before each experimental determination.

For chemical analysis, the films were dissolved in 5 ml of a 1% nitric acid solution and the resultant samples were then analysed by inductively coupled plasma mass spectrometry (ICP-MS). Measurements were made in a Perkin-Elmer spectrometer Elan 6000. Certified standard solutions of cobalt and molybdenum ions containing rhodium as internal standard were used to calibrate the instrument.

Raman measurements were performed at room temperature with a Jobin Yvon T64000 spectrometer coupled with an Olympus metallographic microscope, using the green line of an Ar^+ laser ($\lambda = 514.5$ nm) as excitation light and working in subtractive mode. The dispersive microprobe was constituted by three monocromators. The samples were exposed to laser powers between 4 and 10 mW with spot size was 1 μm.

Auger spectroscopy measurements were done with a PHI 670 scanning Auger nanoprobe system, which allowed a controlled sputtering of the samples and, simultaneously, the in-depth measurement of the chemical composition. The beam energy of the electron gun was selected at 10 kV and with a current of 10 nA. The level of vacuum was kept below 10^{-7} pa. To ensure that measurements were taken in a flat central region of the crater, the sputter area was larger than that scanned by the electron beam.

X-ray photoelectron spectroscopy (XPS) measurements were performed with a PHI 5600 multitechnique system, using standard AlK_α radiation, with a resolution of 0.1 eV.

3. Results

3.1. *Electrochemical study*

A first electrochemical study of the electrodeposition process was performed using solutions with 0.1 mol dm^{-3} Co(II) and different molybdate concentrations ranged between 0 and 0.015 mol dm^{-3}. The voltammetric response (Figure 1) showed that the gradual increase in molybdate concentration in solution advanced the appearance of the sharp reduction current increase, which was related in previous work to the Co–Mo deposition process [11]. When the voltammetric response previous to the onset of alloy deposition was zoomed (picture inside of Figure 1), a zone of low reduction current was detected (zone I) followed by the beginning of alloy deposition (zone II). By increasing the molybdate concentration the current related to zone I was enhanced.

For all solutions, by reversing the negative scan at more negative potentials than those corresponding to the beginning of alloy deposition, a typical nucleation loop was detected. A clear oxidation peak centred between −250 and −300 mV was recorded during the positive scan.

For these solutions, in the chronoamperometric experiments, two distinct shapes of the j/t transient were observed, depending on the applied potential. At low negative potentials, the j/t transients showed a monotonic current increase, even when the deposition time was increased to several hours, with a low charge involved (Figure 2, curves (a) and (b)). Applying more negative potentials, the j/t transients showed an initial zone of relatively low current followed by a sudden slope change (Figure 2, curve (c)). The length of time for

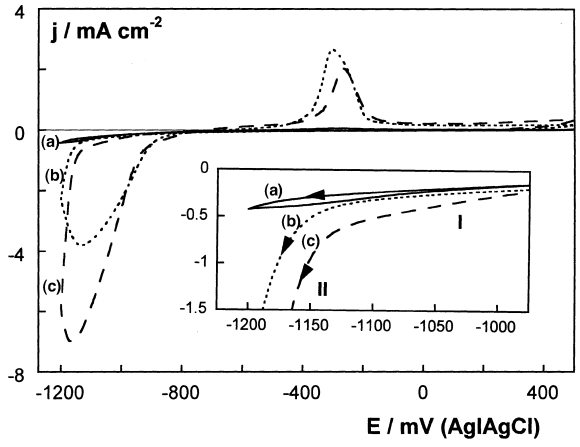

Fig. 1. Cyclic voltammograms of 0.1 mol dm^{-3} $CoSO_4$ + x mol dm^{-3} Na_2MoO_4 + 0.2 mol dm^{-3} $Na_3C_6H_5O_7$ solution. $v = 50$ mV s^{-1}. Cathodic limit −1200 mV. (a) $x = 0$, (b) $x = 0.005$, (c) $x = 0.015$. Under quiescent conditions.

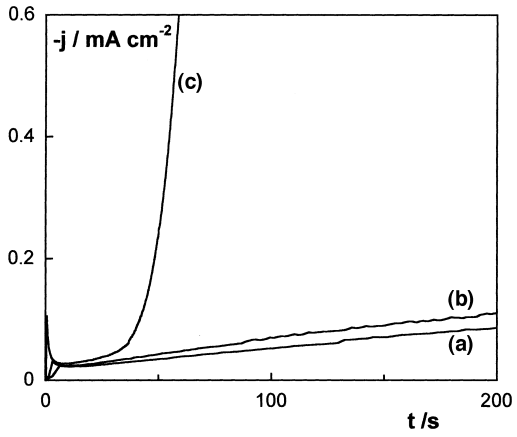

Fig. 2. j/t transients of a 0.1 mol dm^{-3} $CoSO_4$ + 0.012 mol dm^{-3} Na_2MoO_4 + 0.2 mol dm^{-3} $Na_3C_6H_5O_7$ solution. Starting potential −500 mV. Final potential: (a) −950 mV, (b) −960 mV, (c) −1000 mV. $\omega = 60$ rpm.

Table 1. Threshold potential of different electrolytic baths containing 0.2 mol dm^{-3} $C_6H_5Na_3O_7$, 0.1 mol dm^{-3} $CoSO_4$ and a variable molybdate concentration

$[MoO_4^{2-}]$ /mol dm^{-3}	$-E_{threshold}$ /mV
0.005	960
0.012	975
0.015	985
0.018	1000
0.035	1050
0.150	1160

the first zone gradually decreased as the applied potentials were made more negative.

For each bath, a potential value at which the potentiostatic response changed drastically – from the behaviour observed in curves (a) and (b) to the behaviour observed in curve (c) – was found. Therefore, it seemed that a minimum potential value had to be applied to detect the appearance of the sharp current increase during the reduction process. This threshold value was a function of bath composition (Table 1), being more negative as the molybdate concentration in solution increased.

3.2. *Characterization of deposits*

Different samples were prepared potentiostatically from the solutions tested in Section 3.1 applying, for each bath, potentials which were at most, 20 mV more negative than the threshold potential. This narrow range of potential was selected in order to ensure clear observation of the first part of the j/t transient in the chronoamperometric experiments.

When samples obtained at the onset of the second part of the j/t transient (Figure 3A, points (a) and (b)) were imaged by SEM, rounded crystallites distributed homogeneously on the substrate were observed (Figure 3B and C). EDS analysis revealed that the crystallites corresponded to a Co–Mo alloy.

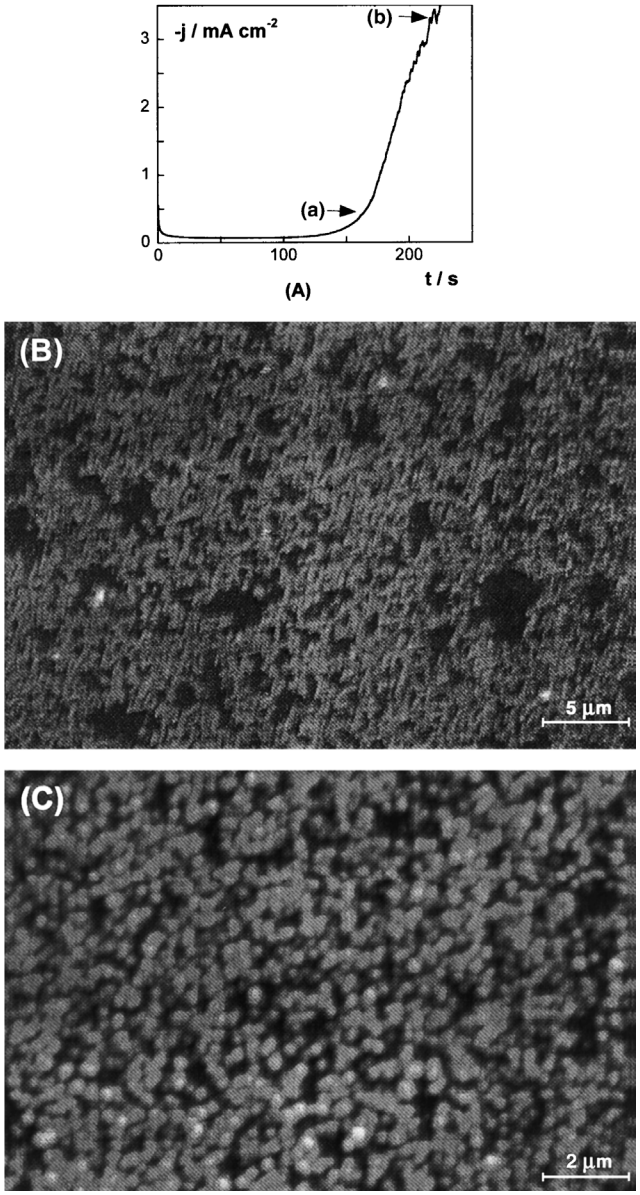

Fig. 3. (A) j/t transient at −980 mV from the solution of Figure 2. (B) and (C) SEM images of deposits corresponding to points (a) and (b) of Figure 3A.

When these images were zoomed between the crystallites, it appeared that a thin film had grown under the nuclei. To characterize this initial film, samples obtained at more positive potentials than the corresponding threshold value were prepared. These potentials were selected to ensure that monotonic j/t transients and long deposition times (thousand seconds) were applied to obtain a sufficient amount of the film (Figure 4A). In these conditions, coloured shiny films were obtained (green, blue or dark red).

SEM micrographs of these samples showed very fine-grained cracked films (Figure 4B). EDS analysis revealed the presence of mainly molybdenum and oxygen, accompanied by a very little cobalt (Figure 4C). Moreover, the significant carbon signal showed that the films were very thin. Chemical ICP-MS analysis of the solutions obtained after dissolving the films corroborated the

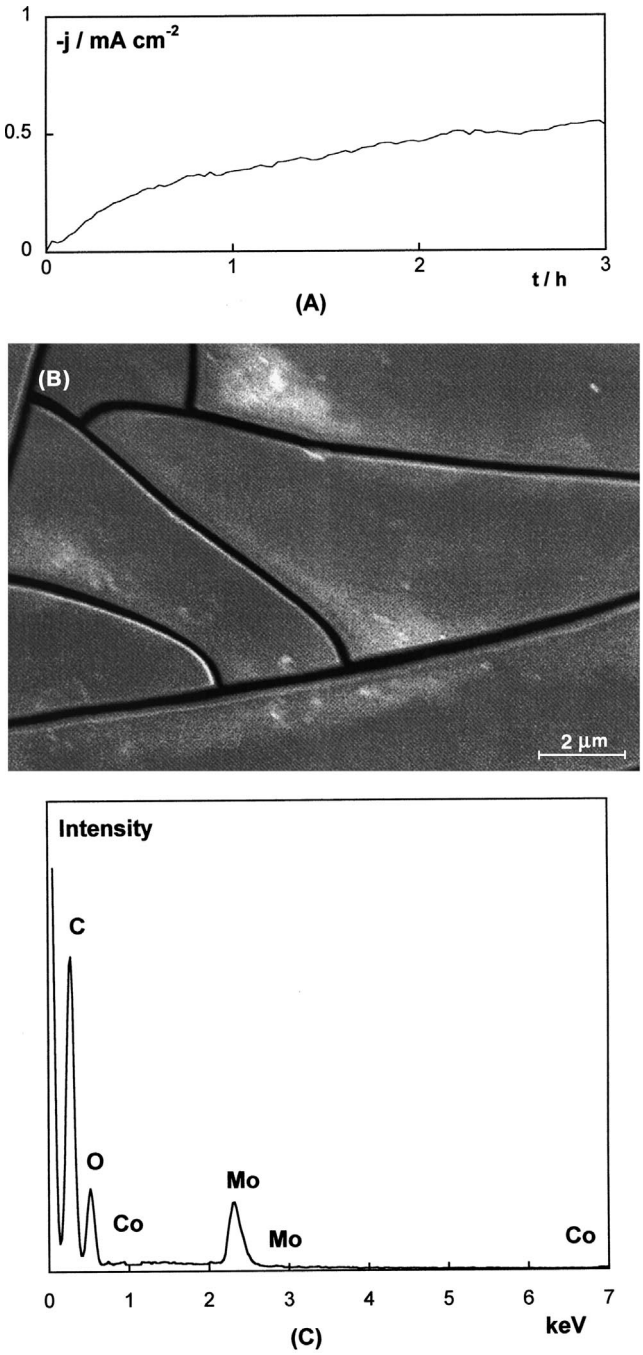

Fig. 4. (A) j/t transient of a film obtained from 0.1 mol dm^{-3} $CoSO_4$ + 0.012 mol dm^{-3} Na_2MoO_4 + 0.2 mol dm^{-3} $Na_3C_6H_5O_7$ solution at −930 mV during 3 h. (B) Corresponding SEM picture of the film. (C) Corresponding EDS microanalysis.

almost unique presence of molybdenum as a metal in these films (Table 2, samples 1–3). Furthermore, ICP-MS analysis revealed that the presence of Co in the deposit increased greatly when the potential applied to produce the film was very close to the corresponding threshold (Table 2, sample 4).

Auger experiments were carried out to characterize the species on the surface. Successive cycles with increasing sputter time were run and the spectra corresponding to the substrate (carbon) and to the three possible elements of the film (cobalt, molybdenum and oxygen) were recorded (Figure 5). These experiments indicated that the film was composed mainly of molybdenum and oxygen, the cobalt signal being at quasi-noise level. Carbon was observed even at low sputtering times due to cracking of the films. Similar results were obtained by XPS measurements (Figure 6).

Table 2. ICP-MS analysis of solutions obtained after dissolving oxide films in 5 ml of 1% nitric acid. The baths employed for preparing the films contained 0.2 mol dm^{-3} $C_6H_5Na_3O_7$, 0.1 mol dm^{-3} $CoSO_4$ and a variable molybdate concentration

Sample	$[MoO_4^{2-}]$ /mol dm^{-3}	$-E$ /mV	ppb Mo	ppb Co
1	0.012	920	152.9	5.9
2		930	140.7	6.8
3	0.035	990	170.3	12.0
4		1040	250.0	90.0

Films were prepared potentiostatically, E being the applied potential.

These analyses indicated that the films were formed of molybdenum oxides/hydroxides. For all the films an apparent atomic Mo:O ratio around 1:1 was obtained from the EDS (Figure 4C) and XPS spectra (Figure 6). In order to explain these unexpected results, similar analyses from standards of stoichiometric molybdenum compounds containing molybdenum and oxygen were performed. For this kind of compound the analyses revealed that, under our experimental conditions, preferential sputtering occurred, leading to a Mo:O lower than the theoretical one. Therefore the stoichiometric Mo:O ratio was not possible to deduce by means of these techniques.

To attempt to clarify the nature of the 'molybdenum oxides' obtained by reduction, before Co–Mo electrodeposition, Raman spectroscopy was used. The Raman spectra of various films showed a similar peak-response and no significant differences attributed to colour were observed (Figure 7A). A broad peak centred on 740 cm^{-1} was recorded for all the samples, and was accompanied by peak/s ranging between 500–580 cm^{-1} (Figure 7A and B, curve (a)). These peaks were clearly related to the presence of molybdenum(IV) oxide in the deposit [12, 13]. The peaks, especially in the interval 500–580 cm^{-1}, were very sensitive to laser power and, after subsequent scans, their definition diminished, being undetectable in some cases. The group of peaks corresponding to Mo(VI) oxide [14] always appeared in the spectra. Their presence was more evident as both the number of scans and the laser power were increased, especially for those that appeared around 950 cm^{-1} and under 250 cm^{-1}.

However, Raman spectra recorded from samples at which cobalt–molybdenum codeposition had been started did not show the peaks, related to Mo(IV) oxide, centred at 740 and 550 cm^{-1} (Figure 7B, curve (b)). A new peak about 660 cm^{-1} appeared, which was possible to assign to Co–Mo interaction [12]. This peak increased in intensity with samples obtained at longer deposition time.

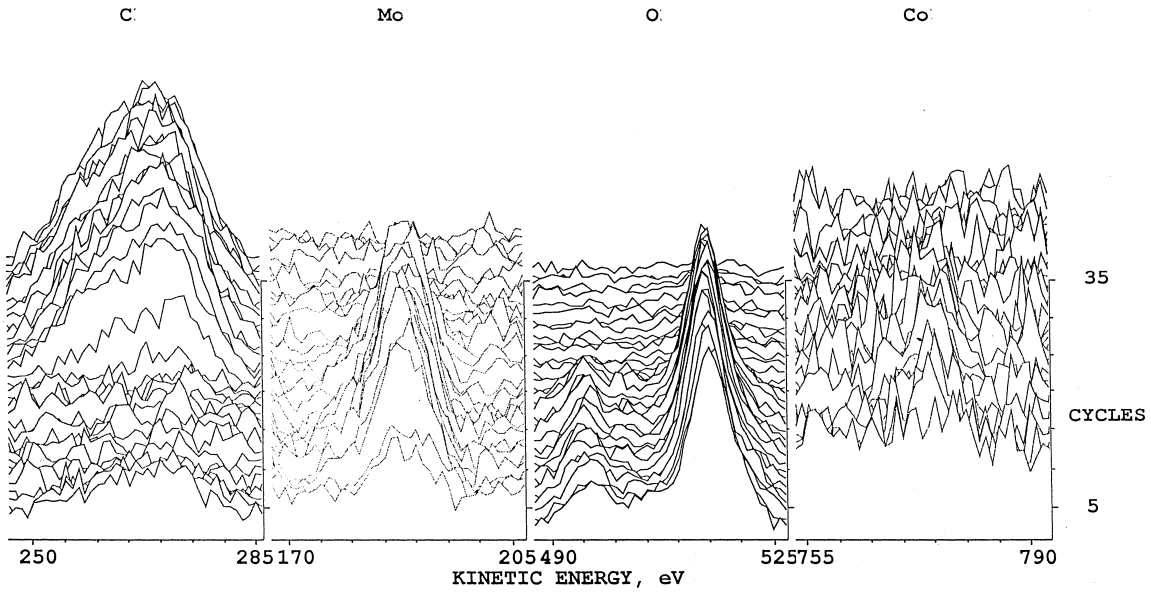

Fig. 5. Auger depth profiles of a film obtained from 0.1 mol dm^{-3} $CoSO_4$ + 0.012 mol dm^{-3} Na_2MoO_4 + 0.2 mol dm^{-3} $Na_3C_6H_5O_7$ solution at −930 mV during 3 h.

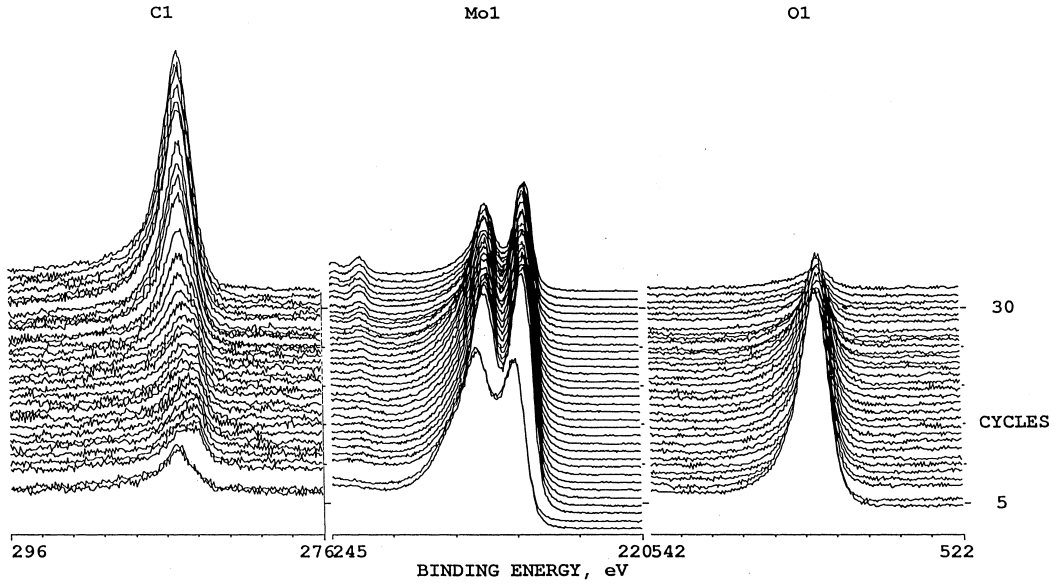

Fig. 6. XPS depth profiles of the same film in Figure 5.

Samples prepared at potentials slightly more positive than the threshold value led, after several hours, to an incipient Co–Mo alloy formation upon the molybdenum oxide film (Figure 8). Obviously, this kind of sample did not correspond to a homogeneous deposit, but they were useful to demonstrate that cobalt–molybdenum deposition took place over the oxide film.

3.3. *Influence of Co(II) concentration on oxide formation*

As the current related to oxide formation increased with increasing molybdate concentration in solution, baths with high molybdate concentrations were tested in order to proceed later to examine the possible influence of Co(II) on molybdenum oxide formation.

Figure 9 shows the voltammetric response when molybdate concentration was raised to 0.15 mol dm^{-3}. During the cathodic scan, a quasi-plateau related to oxide formation appeared (zone I), followed by a sharp reduction current increase (zone II). Reversing the scan, whether at the onset of the second process (curve (a)) or at more negative potentials (curve (b)), a broad oxidation band was recorded from −800 mV. This oxidation current was greatly minimised under stirring conditions. Lengthening the positive scan to more positive potentials, a very small peak around −125 mV was recorded, related to cobalt–molybdenum oxidation. The charge involved in this peak was always very low (i.e., it was not sensitive to the cathodic limit).

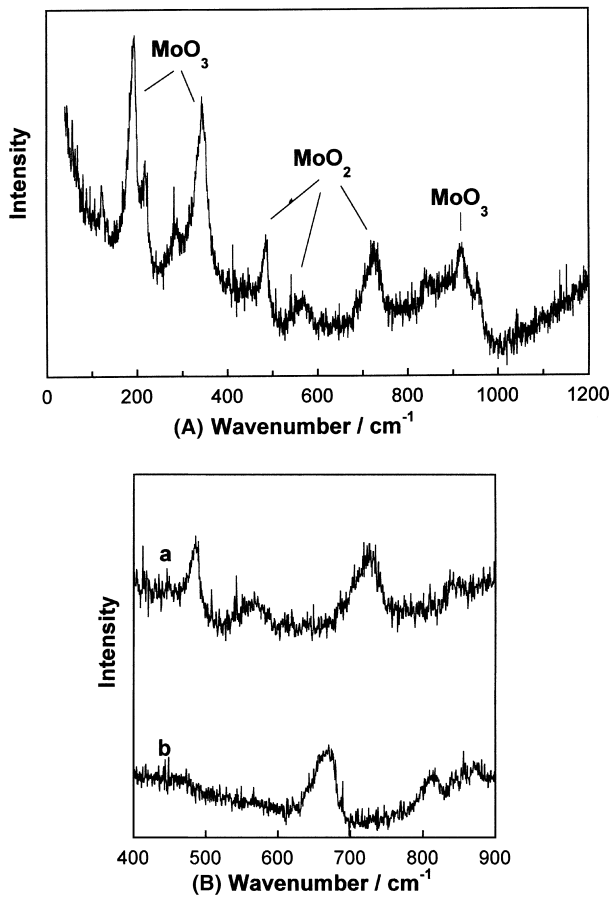

Fig. 7. Raman spectra of the films obtained from: (A) 0.1 mol dm^{-3} $CoSO_4$ + 0.012 mol dm^{-3} Na_2MoO_4 + 0.2 mol dm^{-3} $Na_3C_6H_5O_7$ solution at −930 mV during 3 h. (B) curve (a) zoom detail between 400 cm^{-1} and 900 cm^{-1} of the (A) spectrum. Curve (b): 0.1 mol dm^{-3} $CoSO_4$ + 0.005 mol dm^{-3} Na_2MoO_4 + 0.2 mol dm^{-3} $Na_3C_6H_5O_7$ solution at −980 mV during 1600 s.

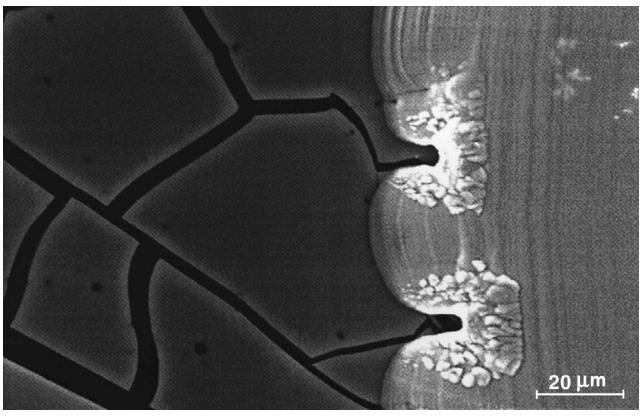

Fig. 8. SEM image of a deposit obtained from the same solution of Figure 2 at −960 mV during 10 h. Left part: molybdenum oxides, right part: Co–Mo alloy, 30% Mo.

The study of Co(II) influence on molybdenum oxides formation was performed at 0.15 mol dm^{-3} MoO_4^{2-}, because the voltammetric plateau ensured a large range of potentials at which only oxide formation occurred. Figure 10 shows a collection of voltammograms recorded from solutions containing a variable Co(II) concentration (between 0 and 0.12 mol dm^{-3}) at fixed cathodic limit of −1100 mV. Voltammetric curves showed that Co(II) in solution clearly favoured the onset of molybdenum oxide formation, this being more evident at concentrations >0.05 mol dm^{-3} (curves (d) and (e)). Only a broad band was recorded during the positive scan and the oxidation charge involved increased with increasing Co(II) concentration.

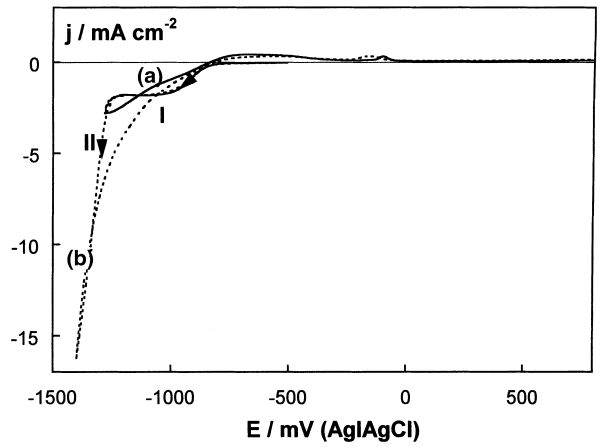

Fig. 9. Cyclic voltammograms of 0.1 mol dm^{-3} $CoSO_4$ + 0.15 mol dm^{-3} Na_2MoO_4 + 0.2 mol dm^{-3} $Na_3C_6H_5O_7$ solution. v = 50 mV s^{-1}. Cathodic limit: (a) −1300 mV, (b) −1400 mV. Under quiescent conditions.

The corresponding chronoamperometric curves, recorded at −900 mV (Figure 11), show, on the one hand a smooth current increase of the j/t transient for Co(II)-free solutions (curve (a)) and a clear enhancement of the reduction process when Co(II) was present in solution (curve (b)). On the other hand, Figure 9 shows that large current densities were reached as Co(II) concentration in solution was increased (curves (b) and (c)).

Various molybdenum oxide films were prepared at low deposition potentials and were compared with those obtained from solutions containing 0.1 mol dm^{-3} $CoSO_4$ (Section 3.2). In contrast to what was observed

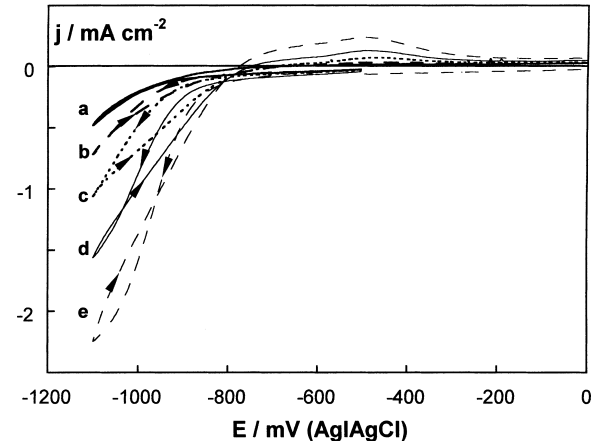

Fig. 10. Cyclic voltammograms of x mol dm^{-3} $CoSO_4$ + 0.15 mol dm^{-3} Na_2MoO_4 + 0.2 mol dm^{-3} $Na_3C_6H_5O_7$ solution. v = 50 mV s^{-1}. Cathodic limit −1100 mV. (a) $x = 0$, (b) $x = 0.024$, (c) $x = 0.045$, (d) $x = 0.065$, (e) $x = 0.085$. Under quiescent conditions.

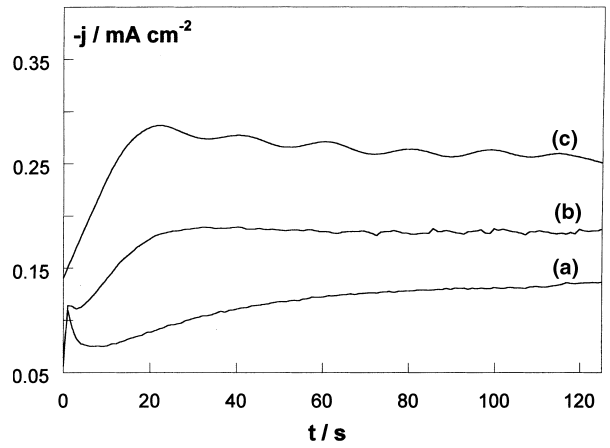

Fig. 11. j/t transients of x mol dm^{-3} $CoSO_4$ + 0.15 mol dm^{-3} Na_2MoO_4 + 0.2 mol dm^{-3} $Na_3C_6H_5O_7$ solution at −900 mV: (a) $x = 0$, (b) $x = 0.024$, (c) $x = 0.045$. Under quiescent conditions.

Table 3. Current efficiency (η) of the molybdenum oxides formation process

$[MoO_4^{2-}]$ /mol dm^{-3}	[Co(II)] /mol dm^{-3}	$-E$ /mV	η /%
0.012	0.1	930	3.8
	0		1.3
	0.1	920	5.3
	0		2.1
0.10	0.1	950	3.1
	0		0.9

Oxide films were prepared potentiostatically from solutions containing 0.2 mol dm^{-3} $C_6H_5Na_3O_7$.

in the first case, films prepared from Co(II)-free solutions were clearly pale-coloured. Table 3 shows the current efficiency of the process involved in preparing molybdenum oxide films. The current efficiency values (η) were deduced by comparing the theoretical reduction charge during deposition with the amount of molybdenum obtained from ICP-MS analysis. The same deposition potential was selected to assure a comparable hydrogen evolution reaction for both kinds of solution, although, in the case of Co(II)-free solutions, it was necessary to increase the deposition time to attain similar deposition charges. The results showed that, at fixed MoO_4^{2-} concentration and applied potential, the efficiency of the process was higher for solutions containing Co(II). However, the low efficiency involved in all cases confirmed that the molybdenum oxide films were very catalytic to hydrogen evolution.

4. Discussion and conclusions

Results obtained have demonstrated that molybdenum(IV) oxides are formed as a first step in induced cobalt–molybdenum codeposition.

A relationship between the electrochemical response during the deposition and the kind of deposit formed on the electrode has been found. The two reduction zones detected in voltammetric experiments are related to molybdenum oxides (zone I) and alloy (zone II) formation, respectively. Chronoamperometric experiments are in agreement with these results. Alloy formation takes place over an initial molybdenum oxide but for Co–Mo alloy deposition a 'threshold potential' is necessary, and at more positive potentials than this critical value, only molybdenum oxides are formed as a consequence of the reduction process.

A combination of the characterisation techniques and the electrochemical studies constitutes a successful way of detecting the previous molybdenum oxide formation during induced cobalt–molybdenum electrodeposition. The SEM shows the formation of a thin film on the electrode substrate, over which cobalt–molybdenum begins to deposit. Results obtained from EDS, Auger and XPS techniques have demonstrated that molybdenum oxides are formed at potentials lower than that for Co–Mo deposition. Molybdenum(IV) oxide formation has been demonstrated by Raman experiments. However, it is not possible to rule out the presence of Mo(VI) oxides, probably produced by oxidation of the freshly deposited molybdenum intermediate oxides.

The coloured molybdenum(IV) oxides obtained at low potentials from Co(II)-molybdate baths may correspond to substoichiometric molybdenum oxides, whose colour is related to the presence of oxygen vacancies [16]. For these oxides an associated intercalation reaction [17] is favoured. During electrochemical formation, ions in solution are inserted into the film (protons, sodium or cobalt ions). When an initial film of molybdenum oxide is formed, significant hydrogen evolution occurs and the possible inclusion of protons may lead to the formation of blue molybdenum oxide [18]. Moreover, the incorporation of some cobalt ions in the films prepared from solutions containing Co(II) may explain their deep colour in comparison to the pale ones obtained from Co(II)-free solutions. At a fixed deposition charge, films produced from Co(II)-free solutions were thinner than those obtained in the presence of Co(II) because of lower current efficiency. In order to discover if colour variation was dependent on film thickness, various samples from Co(II)-free baths were prepared with increasing deposition charge or deposition time. In all cases, films were pale-coloured. Therefore, colour variation could not be solely attributed to film thickness.

At our working pH, $CoCit^-$ is the predominant cobalt(II) species in solution [19, 20]. Then, the formation of molybdenum oxides can be catalysed by the $CoCit^-$ species:

$$MoO_4^{2-} + 2\,H_2O + 2\,e^- \overset{CoCit^-}{\longrightarrow} MoO_2 + 4\,OH^- \qquad (1)$$

The high efficiency of molybdenum oxide formation when Co(II) is present in solution may be related to the simultaneous adsorption of $CoCit^-$ on the molybdenum oxides freshly deposited, thereby reducing the hydrogen evolution.

$$MoO_2 + CoCit^- \longrightarrow [MoO_2 - CoCit^-]_{ads} \quad (2)$$

However, the adsorption of Co(II) over the molybdenum oxide is not enough to promote molybdenum deposition. Only when sufficient potential is applied does the discharge of the molybdenum oxide to molybdenum metal take place.

The detection of the intermediate molybdenum oxides is in agreement with the mechanism proposed by Podlaha et al. for M–Mo electrodeposition [8–10], M being nickel, iron or cobalt, in which the first step is the reduction of MoO_4^{2-} to Mo(IV) by means of the collaboration of M(II)L (L being a ligand) to form an adsorbed intermediate $[M(II)(L)MoO_2]_{ads}$ species. Next, the formation of the Co–Mo alloy occurs through steps in which $CoCit^-$ is reduced to cobalt and $[MoO_2–CoCit^-]_{ads}$ is reduced to molybdenum.

$$CoCit^- + 2\,e^- \longrightarrow Co + Cit^{3-} \quad (3)$$

$$[MoO_2–CoCit^-]_{ads} + 2\,H_2O + 4\,e^- \longrightarrow Mo + CoCit^- + 4\,OH^- \quad (4)$$

At low molybdate concentration, alloy deposition occurs at more positive potentials than those corresponding to pure cobalt [11], probably because of the greater facility of cobalt to be deposited on the molybdenum oxides than on vitreous carbon. However, when the molybdate concentration is increased, the threshold potential is shifted to more negative values. This potential shift may be explained by the semiconducting nature of these molybdenum oxides. With increasing molybdate concentration in solution thicker molybdenum oxide films are formed, thereby making Co–Mo deposition more difficult. Moreover, as a result of the threshold potential shift, a greater hydrogen coevolution accompanies alloy deposition.

Depending on the counterbalance between the concentration of electrolyte and the deposition parameters, either Co–Mo deposits or molybdenum oxide films may be obtained. Although only a low current efficiency achieved during electrochemical preparation of oxide films, electrochemistry may constitute an alternative to physical methods like sputtering and PVD.

Acknowledgements

The authors thank the Serveis Cientificotècnics (Universitat de Barcelona) for the use of their equipment. This paper was supported financially by contract MAT 2000-0986 from the Comisión Interministerial de Ciencia y Tecnología (CICYT) and by the Comissionat of the Generalitat de Catalunya under Research Project 2001SGR00046. E. Pellicer also thanks the DURSI of the Generalitat de Catalunya for financial support.

References

1. Ch . Fan, D.L. Piron, A. Sleb and P. Paradis, *J. Electrochem. Soc.* **141** (1994) 382.
2. Ch. Fan, D.L. Piron and P. Paradis, *Electrochim. Acta* **39** (1994) 2715.
3. E. Chassaing, M.P. Roumegas and M.F. Trichet, *J. Appl. Electrochem.* **25** (1995) 667.
4. Ch. Chu and S. Wu, *J. Electrochem. Soc.* **147** (2000) 2190.
5. A. Brenner, 'Electrodeposition of Alloys', vols. 1 and 2 (Academic Press, New York, 1963).
6. H. Fukushima, T. Akiyama, S. Akagi and K. Higashi, *Trans Jpn. Inst. Met.* **20** (1979) 358.
7. E. Chassaing, K. Vu Quang and R. Wiart, *J. Appl. Electrochem.* **19** (1989) 839.
8. E.J. Podlaha and D. Landolt, *J. Electrochem. Soc.* **143** (1996) 885.
9. E.J. Podlaha and D. Landolt, *J. Electrochem. Soc.* **143** (1996) 893.
10. E.J. Podlaha and D. Landolt, *J. Electrochem. Soc.* **144** (1997) 1672.
11. E. Gómez, E. Pellicer and E. Vallés, *J. Electroanal. Chem.* **517** (2001) 109.
12. Z.J. Niu, S.B. Yao and S.M. Zhou, *J. Electroanal. Chem.* **455** (1998) 205.
13. Y. Zeng, Z. Li, M. Ma and S. Zhou, *Electrochem. Commun.* **2** (2000) 36.
14. T. Ivanova, K.A. Gesheva and A. Szekeres, *J. Solid Stat. Electrochem.* **6** (2002) [online March 8].
15. P. Garrido, E. Gómez and E. Vallés, *J. Electroanal. Chem.* **441** (1998) 147.
16. V.K. Sabhapathi, M. Hussain, P.S. Reddy, P. Ramakrishna Reddy, S. Uthanna, B.S. Naidu and P. Jayarama Reddy, *Phys. Status Solidi (a)* **148** (1995) 167.
17. J. Scarminio, A. Lourenço and A. Gorenstein, *Thin Solid Films* **302** (1997) 66.
18. S. Liu, Q. Zhang, E. Wang and S. Dong, *Electrochem. Comm.* **1** (1999) 365.
19. S.S. El Rehim, S.M. El Wahaab, M.A.M. Ibrahim and M.M. Dankeria, *J. Chem. Technol. Biotechnol.* **73** (1998) 369.
20. D.R. Lide (Ed.), 'Handbook of Chemistry and Physics', 77th edn. (CRC Press New York, 1996–1997), pp. 8–50.